Title: The feedback between selection and demography shapes genomic diversity during coevolution

Authors: Cas Retel[1,2]†, Vienna Kowallik[3,4]†, Weini Huang[5,6], Benjamin Werner[7], Sven Künzel[8], Lutz Becks[3,9,10]‡, Philine G.D. Feulner[1,2]*‡

Affiliations:

[1]Department of Fish Ecology and Evolution, Center for Ecology, Evolution and Biogeochemistry, EAWAG, Swiss Federal Institute of Aquatic Science and Technology, Kastanienbaum, Switzerland.

[2]Division of Aquatic Ecology, Institute of Ecology and Evolution, University of Bern, Bern, Switzerland.

[3]Community Dynamics Group, Dept. Evolutionary Ecology, Max Planck Institute for Evolutionary Biology, Plön, Germany.

[4]Current address: Okinawa Institute of Science and Technology | OIST · Ecology and Evolution Unit.

[5]Group of Theoretical Biology, The State Key Laboratory of Biocontrol, School of Life Science, Sun Yat-sen University, Guangzhou, China.

[6]Complex Systems and Networks Research Group, School of Mathematical Sciences, Queen Mary University of London, United Kingdom.

[7]Evolutionary Genomics and Modelling Lab, Centre for Evolution and Cancer, The Institute of Cancer Research, London, United Kingdom.

[8]Dept. Evolutionary Genetics, Max Planck Institute for Evolutionary Biology, Plön, Germany.

[9]Kiel Evolution Center, Biologiezentrum, Kiel, Germany.

[10]Current address: Limnological Institute University Konstanz, Aquatic Ecology and Evolution. Konstanz, Germany.

* Correspondence to: philine.feulner@eawag.ch.

† Equal contribution.

‡ Equal contribution.

Abstract: Species interactions and coevolution are integral to ecological communities, but we lack empirical information on when and how such interactions generate and purge genetic diversity. Using genomic time-series data from host-virus experiments, we found that coevolution occurs through consecutive selective sweeps in both species, with temporal consistency across replicates. Sweeps were accompanied by phenotypic change (resistance or infectivity increases) and expansions in population size. In the host, population expansion enabled rapid generation of genetic diversity in accordance with neutral processes. Viral molecular evolution was in contrast confined to few genes, all putative targets of selection. This study demonstrates that molecular evolution during species interactions is shaped by both eco-evolutionary feedback dynamics and interspecific differences in how genetic diversity is generated and maintained.

One Sentence Summary: Rapid genomic changes during a coevolutionary arms race highlight the reciprocal effects of ecology and evolution.

Main Text: Host-pathogen interactions are commonplace and play a major role in many ecological and evolutionary processes (*1*, *2*), affecting the pace of molecular evolution (*3*) and rates of diversification and speciation (*4*). When species coevolve, the selection they impose on each other is temporally variable (*5*). Coevolutionary dynamics of hosts and parasites are traditionally placed on a spectrum between two extremes, where evolutionary changes are either driven by recurrent consecutive fixations of beneficial novel genotypes (Arms Race dynamics) or by non-constant selection maintaining the presence of multiple co-existing genotypes (Fluctuating-Selection dynamics) (*6–9*). To fully understand the effects of coevolutionary interactions on community composition, ecosystem stability and biodiversity, temporally resolved information for both antagonists (*10*) is essential to quantify how selection varies through time (*11*).

During coevolution, selection imposed by the antagonist varies depending on abundances of both interacting partners. Rapid evolution of traits with which species interact decreases the performance of antagonists and can hence affect population sizes (*12*). Because antagonist's encounter rates depend on density, changes in population size alter the strength and sometimes direction of selection (*13*), giving rise to a feedback between evolutionary and ecological change (*14*). This can lead to deviations from traditional coevolutionary expectations (*15*, *16*) and can affect molecular evolution (*17*), with so far unknown consequences for the build-up, maintenance and purging of genetic diversity (*18*).

Time-resolved imaging of genomic change in large microbial populations shows that high mutation supply can make molecular evolution under constant selection surprisingly multifarious (*19*, *20*). In such populations, *de novo* mutations generate variation rapidly enough for beneficial alleles to be common. This causes clonal interference of beneficial mutations

within populations (*21*, *22*) and genetic hitchhiking, where selection acting on a mutation of large phenotypic effect influences the frequency trajectories of physically linked mutations with no or smaller effects (*23*, *24*). In the absence of recombination, populations are an assembly of coexisting genotypes with comparable fitness (*25*). Genotypes continuously acquire beneficial mutations, and genotypes with higher fitness than the population average tend to increase in frequency (*26*). Experiments have shown that dynamics of population-wide genetic diversity are remarkably reproducible, but rare highly beneficial combinations of mutations can cause stochastic crashes in genetic diversity (*27*). Constant environmental selection over longer evolutionary timescale results in predictable fitness increase and the frequent occurrence of adaptive mutations in the same genes, while their temporal changes in frequency vary considerably between replicates (*20*).

To assess the effect of an eco-evolutionary feedback on the temporal dynamics of genome-wide molecular evolution in a host-parasite system, we ran an experimental evolution study using initially isogenic algal host (*Chlorella variabilis* strain NC64A) and initially isogenic dsDNA virus (PBCV-1) in replicated chemostat systems (n=3) and tracked genomic, phenotypic and population size changes of host and virus populations over time (100 days ~ 100 generations). Both species reproduce exclusively asexually. Similar to previous experiments with this system (*17*, *28*), we observed initial damped cycling of host and virus population sizes of two orders of magnitude, which changed to more stable population dynamics without cycling around day 57-75 (Fig. 1A). These dynamics were highly repeatable across replicates with a phase shift of 0.09±0.4 days between the replicates (mean±sd). We followed coevolution on the phenotypic level through time-shift experiments, by isolating host clones from ten time points and exposing them to past, contemporary and future virus populations from the same chemostat

replicate. We observed three rounds of increases in host resistance range (i.e. proportion of virus populations a host clone is resistant to) and two rounds of increases in virus infectivity range (i.e. proportion of host clones a virus population is able to infect; Fig. 1B, Fig. S1). Host fitness (i.e. growth rate in presence of contemporary virus) increased and decreased in concert with these phenotypic changes (Fig. S2). As in previous experiments with this system, host and virus coevolved asymmetrically with the evolution of a generalist resistant host (host individuals resistant to virus from every time point) (*28*) at days 57 or 75. The evolution of the generalist led to a shift from Arms Race dynamics to Fluctuating Selection dynamics, where population dynamics stabilised and maintenance of variation in the host populations was driven by the cost of increasing resistance (Figures S3 and S4) (*28*). Since the coevolutionary response of *Chlorella* resulted in reduced growth rates, the interactions studied here inevitably affect ecosystem functioning of a relevant primary producer in freshwater lakes. In summary, the antagonistic species interaction resulted in highly variable ecological dynamics over time.

We demonstrate changes in strength of the ecological interaction between the two antagonists by categorising the time intervals as one of two classes: i) periods when virus infectivity was higher than or equal to host resistance, when encounters between antagonistic individuals likely led to infection (= phenotypic match), and ii) periods characterised by higher resistance range, when encounters rarely resulted in infection events (= phenotypic mismatch; Fig. 1C). In intervals with a phenotypic match, selection for host resistance was strong, while we expect virus populations to increase in size. A phenotypic mismatch on the other hand warrants pressure on the virus populations to evolve new means of infectivity, while it allows the host to grow without antagonistic restraints. Experiments started with a phenotypic match, then match

and mismatch alternated during the Arms Race phase, followed by a phenotypic mismatch in the Fluctuating Selection phase.

To follow evolutionary change on the genome level, we sequenced whole-genomes of samples from ten time points for each replicate to obtain population data (Pool-seq) for both species simultaneously. For analysis, we exclusively focused on single nucleotide polymorphisms (SNPs) absent from the ancestral population that reached appreciable frequencies (due to differences in sequences coverage, frequencies < 0.05 in the virus and < 0.25 in the host are not unambiguously distinguishable from sequencing errors) at more than one time point; hereafter called derived alleles (Table S1). Hence, the genomic change presented excludes various technical artefacts and low-frequency variants, but adequately represents the variation governed by selection and selective interferences.

Rapid genetic changes were observed in both species, but dynamics of molecular change play out differently in the two species. (Fig. 1D,E). The total number of derived alleles per replicate was 388±83 and 9±2 (mean±sd, number of replicates is three) in the host and virus populations, respectively. In the host populations more than half of the observed mutations (211±55) were synonymous or occurred in intergenic regions (Fig. 2B). The majority of such changes have no or minor phenotypic effects, suggesting that their substantial allele frequency changes are rather due to a physical association with mutations of larger selective advantage (genetic hitchhiking) (*23*). In contrast, the majority of the SNPs observed in the virus populations (20 out of 21 unique SNPs) were non-synonymous, meaning that they are likely candidates driving the coevolutionary dynamics rather than hitchhiking on an adaptive background. A small genome densely packed with protein-coding regions, skewed offspring distributions and stronger purifying selection all contribute to the lack of genetic hitchhiking in viral evolution (*29*).

Our temporal resolution allowed us to detect the signature of a selective sweep in the host populations at two time points. In every replicate, within-population diversity (Fig. 3) markedly dropped in the time intervals preceding days 27 and 64. Such a diversity reduction is characteristic for a selective sweep, when a low-frequency beneficial mutation quickly rises to fixation and physically linked variants are dragged along, eliminating genetic variation (*30*). During sweeps, the host populations became genetically more similar to the ancestor (Fig. S6). The observation and timing of these selective sweeps reinforces previous conclusions based on phenotypic changes that the coevolutionary system is governed by Arms Race dynamics until the generalist host evolves (Fig. 1) (*28*).

The allele frequency spectra per time point can be used to assess within-population structure. The classic Luria-Delbrück model predicts that within an expanding cohort of equally fit cells, the allele frequency spectrum of *de novo* variants can be described by a simple power-law distribution (*31*, *32*). Such a dependency can be observed when neutral *de novo* mutation occurs at a reasonably high rate, which is expected for *Chlorella* with a genome size of 42 Mb (see Methods for more details). This allows us to separate time points when the host population consists of one cohort all carrying an acquired highly beneficial mutation, from time points when populations consist of multiple coexisting cohorts. In the first case, the observed genetic variation is shaped primarily by neutral evolutionary processes (expansion), while in the latter, frequency changes are also driven by interference between mutations of moderate effects that segregate in the different cohorts.

Examination of the host allele frequency spectrum of derived alleles per time point revealed a power law dependence at the same time points when genome-wide diversity was reduced (Fig. S5; additional time point in in replicate III at day 12). Regressing the presence of

this dependence on host population growth rate in the three days leading up to the corresponding time point revealed a positive correlation (generalized mixed effect model with family binomial and replicate as random effect: z= 2.175, p= 0.0297; Fig. 3B). This suggests that matches to the Luria-Delbrück model follow host expansion phases. Thus, only directly after a sweep did host populations consist of one expanding cohort, and the observed rapid (re)generation of genetic variation is facilitated by this expansion (Fig. 1).

A first sweep in the virus populations occurred directly after the first host sweep between days 29 and 41. After none of the derived variants showed noticeable frequency changes across the first three time points sampled, a previously undetected variant increased in frequency over 70% in this time interval in every replicate. This first sweeping allele did not go to fixation in any of the replicates, however such a dramatic frequency change (>70% in ~12 generations) implies a large selection coefficient (0.90±0.35, mean±sd across three replicates). The ecological impacts of this first virus sweep were virus population growth, host decline and the interaction reverted to a phenotypic match (Fig. 1C). After evolution of a generalist host, species interaction strength remained low because the majority of host cells were resistant to the contemporary virus population (Fig. S1) and the coevolutionary system then switched to Fluctuating Selection dynamics (Fig. S2) (*28*). Derived viral alleles both substantially increased and decreased in frequency and patterns of genomic change were less similar between replicates than the ecological dynamics.

In the host populations, 294 out of a total of 703 SNPs were found multiple times and 166 occurred in all three replicates (Fig. 4B). The probability of observing the same mutation more than once by chance is small (Table S2), hence suggestive of the action of natural selection. More than half of the repeated mutations (219±35) were already observed before the introduction

of the virus at day 12, and they might provide a benefit in the abiotic environment or during competitive growth rather than confer resistance. We expect variants in genes impacting resistance to increase in frequency at time intervals leading up to those time points where sweeps were detected, and evaluated which SNPs fit this criterium. Potential candidate genes for the evolution of resistance are genes affecting outer cell wall composition, alterations of which would prevent viral recognition of the host cell. However, we found no primary candidate genes amongst the high-frequency and repeatedly found SNPs at days 27 and 64 (Tables S3 and S4). This could be because resistance was encoded by a larger structural variant (*17*) which we do not evaluate here. Also, cell walls and the extracellular matrix are complex biological structures regulated by many genes, and it is quite conceivable that different mutations have similar phenotypic outcomes, or that the evolution of resistance is mediated by multiple mutations of moderate effect.

In the virus populations, five out of 21 unique mutations were observed in more than one replicate (Fig. 4B,C). All five were non-synonymous and three of them - among which the one mutation observed in every replicate - altered the protein structure of the gene *A540L*, which is highly conserved within the 41 Chlorovirus isolates sequenced to date (*33*). A fourth mutation was in the gene *A122R*. Both these genes have no known orthologs outside the family of Chloroviruses and are expressed during late-infection stage, i.e. after viral DNA synthesis has begun (*34*). The fifth mutation was in the first glycosyltransferase-domain of the gene *A064R*, encoding for a large protein present in every Chlorovirus sequenced so far (*33*). The protein encoded for by *A064R* plays an important role in construction of the major capsid glycoprotein that makes up the outer virus particle; PBCV-1 mutants possessing a truncated version of the gene are viable but less stable (*35*). The functional annotations and high degree of conservation

of these three repeatedly mutated genes support the notion that the mutations we detect in the virus were driving the observed dynamics rather than genetic hitchhikers.

Adaptation by natural selection is based on the premise that genetic variation which enhances reproductive success increases in frequency over generations. Here, we have documented such frequency change on a fine temporal scale, in an experimental system comprising two species that are each other's primary selective agent. We identified signatures of adaptive sweeps with temporal consistency in both host and virus, but the genome-wide patterns of molecular evolution differed markedly between the species. Viral evolution was confined to mutations in three candidate genes for infectivity evolution, which are all specific to and highly conserved among Chloroviruses. In contrast, *de novo* mutation rapidly generated variation in the host populations in between sweeps, which erased diversity at comparable timescales.

We identified adaptive sweeps in the host by the loss of genetic diversity and linked those to increases in resistance. The concurrent change in species interaction strength allowed the host populations to expand, which facilitated the rapid build-up of genetic diversity - until the virus counter-adapted. Thus, evolution was both a cause (increased resistance) and a consequence (neutral diversity build-up) of ecological change (population expansion). Our results demonstrate how both eco-evolutionary feedback dynamics and interspecific differences in substitution supply rate between the species influence molecular change during host-pathogen coevolution. We anticipate that a more widespread recognition of the various ways by which ecological and evolutionary change can affect each other will be essential to interpret the genomic signature of evolution under species interactions and understand the mode, pace, and predictability of evolution in natural communities.

References and Notes:

1. J. N. Thompson, *The Geographic Mosaic of Coevolution* (University of Chicago Press, ed. 1, 2005).

2. M. A. Brockhurst *et al.*, Running with the Red Queen: the role of biotic conflicts in evolution. *Proc. R. Soc. B*. **281**, 1–9 (2014).

3. A. Betts, C. Gray, M. Zelek, R. C. MacLean, K. C. King, High parasite diversity accelerates host adaptation and diversification. *Science (80).* **360**, 907–911 (2018).

4. T. L. Parchman, C. A. Buerkle, V. Soria-Carrasco, C. W. Benkman, Genome divergence and diversification within a geographic mosaic of coevolution. *Mol. Ecol.* (2016), doi:10.1111/mec.13825.

5. D. H. Janzen, When is it coevolution? *Evolution (N. Y).* **34** (1980), pp. 611–612.

6. M. E. J. Woolhouse, J. P. Webster, E. Domingo, B. Charlesworth, B. R. Levin, Biological and biomedical implications of the co-evolution of pathogens and their hosts. *Nat. Genet.* **32**, 569–577 (2002).

7. A. Agrawal, C. M. Lively, Infection genetics: gene-for-gene versus matching-alleles models and all points in between. *Evol. Ecol. Res.* **4**, 79–90 (2002).

8. S. E. Forde *et al.*, Understanding the limits to generalizability of experimental evolutionary models. *Nature*. **455**, 220–223 (2008).

9. A. Tellier, S. Moreno-Gámez, W. Stephan, Speed of adaptation and genomic footprints of host-parasite coevolution under arms race and trench warfare dynamics. *Evolution (N. Y).* **68**, 2211–2224 (2014).

10. A. Papkou *et al.*, The genomic basis of Red Queen dynamics during rapid reciprocal host-pathogen coevolution. *Proc. Natl. Acad. Sci. U. S. A.*, 201810402 (2018).

11. S. F. Bailey, T. Bataillon, Can the experimental evolution programme help us elucidate the genetic basis of adaptation in nature? *Mol. Ecol.* **25**, 203–218 (2016).

12. T. Yoshida, L. E. Jones, S. P. Ellner, G. F. Fussmann, N. G. Hairston Jr, Rapid evolution drives ecological dynamics in a predator–prey system. *Nature*. **424**, 303–306 (2003).

13. A. Papkou, C. S. Gokhale, A. Traulsen, H. Schulenburg, Host–parasite coevolution: Why changing population size matters. *Zoology*. **119**, 330–338 (2016).

14. T. W. Schoener, The Newest Synthesis: Understanding the interplay of evolutionary and ecological dynamics. *Science (80).*, 426–429 (2011).

15. Y. Song, C. S. Gokhale, A. Papkou, H. Schulenburg, A. Traulsen, Host-parasite coevolution in populations of constant and variable size. *BMC Evol. Biol.* **15**, 1–15 (2015).

16. E. Van Velzen, U. Gaedke, Disentangling eco-evolutionary dynamics of predator-prey coevolution: the case of antiphase cycles. *Sci. Rep.* **7**, 17125 (2017).

17. J. Frickel, P. G. D. Feulner, E. Karakoc, L. Becks, Population size changes and selection drive patterns of parallel evolution in a host–virus system. *Nat. Commun.* **9**, 1706 (2018).

18. P. W. Messer, S. P. Ellner, N. G. Hairston, Can population genetics adapt to rapid evolution? *Trends Genet.* **32**, 408–418 (2016).

19. I. Cvijović, A. N. Nguyen Ba, M. M. Desai, Experimental studies of evolutionary dynamics in microbes. *Trends Genet.* **34**, 1–11 (2018).

20. B. H. Good, M. J. McDonald, J. E. Barrick, R. E. Lenski, M. M. Desai, The dynamics of

molecular evolution over 60,000 generations. *Nature*. **551**, 45–50 (2017).

21. P. J. Gerrish, R. E. Lenski, The fate of competing beneficial mutations in an asexual population. *Genetica*. **102–103**, 127–144 (1998).

22. G. I. Lang, D. Botstein, M. M. Desai, Genetic variation and the fate of beneficial mutations in asexual populations. *Genetics*. **188**, 647–661 (2011).

23. S. Schiffels, G. J. Szöllosi, V. Mustonen, M. Lässig, Emergent neutrality in adaptive asexual evolution. *Genetics*. **189**, 1361–1375 (2011).

24. G. I. Lang *et al.*, Pervasive genetic hitchhiking and clonal interference in forty evolving yeast populations. *Nature*. **500**, 571–574 (2013).

25. I. M. Rouzine, J. Wakeley, J. M. Coffin, The solitary wave of asexual evolution. *PNAS*. **100**, 587–592 (2003).

26. M. M. Desai, D. S. Fisher, Beneficial mutation-selection balance and the effect of linkage on positive selection. *Genetics*. **176**, 1759–1798 (2007).

27. J. R. Blundell *et al.*, The dynamics of adaptive genetic diversity during the early stages of clonal evolution. *Nat. Ecol. Evol.* **3**, 293–301 (2019).

28. J. Frickel, M. Sieber, L. Becks, Eco-evolutionary dynamics in a coevolving host–virus system. *Ecol. Lett.* **19**, 1–31 (2016).

29. K. K. Irwin *et al.*, On the importance of skewed offspring distributions and background selection in virus population genetics. *Heredity (Edinb)*. **117**, 393–399 (2016).

30. N. H. Barton, The effect of hitch-hiking on neutral genealogies. *Genet. Res. (Camb)*. **72**, 123–133 (1998).

31. M. J. Williams, B. Werner, C. P. Barnes, T. A. Graham, A. Sottoriva, Identification of neutral tumor evolution across cancer types. *Nat. Genet.* **48**, 238–244 (2016).

32. D. A. Kessler, H. Levine, Large population solution of the stochastic Luria-Delbrück evolution model. *Proc. Natl. Acad. Sci.* **110**, 11682–11687 (2013).

33. A. Jeanniard *et al.*, Towards defining the chloroviruses: a genomic journey through a genus of large DNA viruses. *BMC Genomics*. **14**, 158 (2013).

34. G. M. Yanai-Balser *et al.*, Microarray analysis of *Paramecium bursaria* Chlorella Virus 1 transcription. *J. Virol.* **84**, 532–42 (2010).

35. C. De Castro *et al.*, Structure of the chlorovirus PBCV-1 major capsid glycoprotein determined by combining crystallographic and carbohydrate molecular modeling approaches. *Proc. Natl. Acad. Sci.*, 201613432 (2017).

36. C. P. D. Brussaard, Optimization of procedures for counting viruses by flow cytometry. *Appl. Environ. Microbiol.* **70**, 1506–1513 (2004).

37. R Core Team, *R: A Language and Environment for Statistical Computing* (Vienna, Australia, 2008; http://www.r-project.org/).

38. C. Torrence, G. P. Compo, A practical guide to wavelet analysis. *Bull. Amer. Meteor. Soc.* **79**, 61–78 (2016).

39. A. Roesch, H. Schmidbauer, WaveletComp: computational wavelet analysis. R package version 1.0. URL https://cran.r-project.org/package=WaveletComp (2014), (available at https://cran.r-project.org/package=WaveletComp).

40. A. M. Bolger, M. Lohse, B. Usadel, Trimmomatic: a flexible trimmer for Illumina sequence data. *Bioinformatics*. **30**, 2114–2120 (2014).

41. H. Li, R. Durbin, Fast and accurate short read alignment with Burrows-Wheeler transform. *Bioinformatics*. **25**, 1754–1760 (2009).

42. G. Blanc *et al.*, The *Chlorella variabilis* NC64A genome reveals adaptation to photosymbiosis, coevolution with viruses, and cryptic sex. *Plant Cell*. **22**, 2943–55 (2010).

43. H. Li *et al.*, The Sequence Alignment/Map format and SAMtools. *Bioinformatics*. **25**, 2078–2079 (2009).

44. R. Kofler, R. V. Pandey, C. Schlötterer, PoPoolation2: Identifying differentiation between populations using sequencing of pooled DNA samples (Pool-Seq). *Bioinformatics*. **27**, 3435–3436 (2011).

45. M. J. McDonald, D. P. Rice, M. M. Desai, Sex speeds adaptation by altering the dynamics of molecular evolution. *Nature*. **531**, 233–236 (2016).

46. R. Kofler, C. Schlötterer, A guide for the design of evolve and resequencing studies. *Mol. Biol. Evol.* **31**, 474–483 (2014).

47. P. Cingolani *et al.*, A program for annotating and predicting the effects of single nucleotide polymorphisms, SnpEff. *Fly (Austin)*. **6**, 80–92 (2012).

48. J. H. Gillespie, *Population genetics - A concise guide* (1998).

49. M. J. Wiser, N. Ribeck, R. E. Lenski, Long-term dynamics of adaptation in asexual populations. *Science (80)*. **342**, 1364–1367 (2013).

50. S. Luria, M. Delbrück, Mutations of bacteria from virus sensitivity to virus resistance. *Genetics*. **28**, 491–511 (1943).

51. D. Bates, B. M. Bolker, M. Mächler, S. C. Walker, Fitting linear mixed-effects models using lme4. *J. Stat. Softw.* **67** (2015), doi:10.18637/jss.v067.i01.

52. L. Van Valen, A new evolutionary law. *Evol. Theory*. **1**, 1–30 (1973).

Acknowledgments: We are grateful to the sequencing team at the MPI in Plön for assistance and to Gulia Bartolomucci for help with collecting phenotypic data. Genomic data analysis for this paper was supported by collaboration with the Genetic Diversity Centre (GDC), ETH Zurich. We thank B. Matthews, H. Maerkle, J. Slate, and N. G. Hairston Jr. for helpful feedback on a previous draft of the manuscript. **Funding:** This work was supported by grants from the German Research Foundation (DFG) to LB (grant BE 4135/3-1, 4135/9) and from the Swiss National Science Foundation (SNSF) to PGDF (grant 310030E-160812 / 1). **Author contributions:** LB and PGDF conceived and designed the study; VK carried out the experiments and collected data; SK performed the sequencing; CR processed and analysed the sequence data; WH and BW ran the coalescence simulations and analysed allele frequency spectra; CR together with LB and PGDF interpreted the results and wrote the manuscript. All authors contributed to and revised the final version of the manuscript. **Competing interests:** The authors declare no competing interests. **Data and materials availability:** Population size counts, phenotypic assays, and filtered derived allele frequencies reported are available as supplementary materials. Raw sequence data will be deposited at SRA. R scripts to conduct the genomic filtering steps are available at github.com/ RetelC/TempDynamics_HostVirCoevol.

Supplementary Materials:

Materials and Methods

Figures S1-S6

Tables S1-S4

Data S1-S3

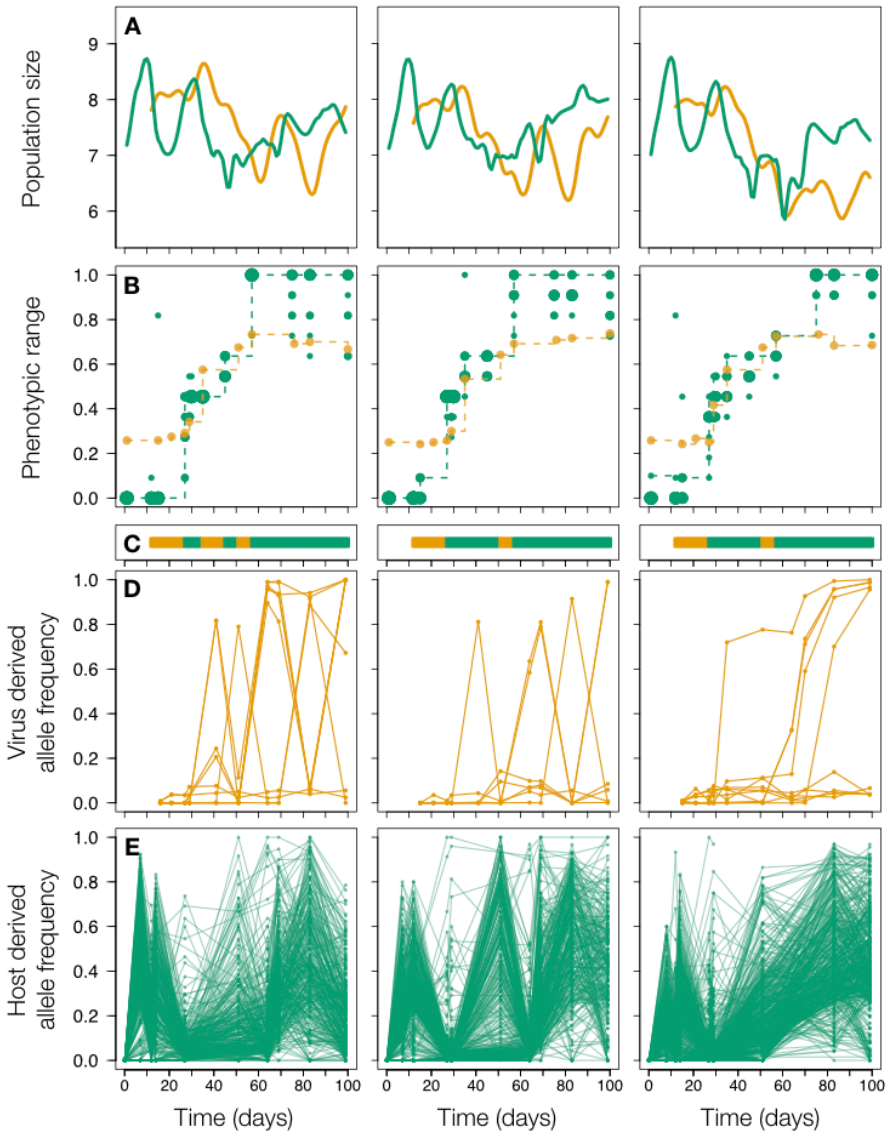

Fig. 1. Ecological and evolutionary change of coevolving host and virus populations. The three columns correspond to three replicate experiments. (**A**) Population sizes of host (green) and virus (orange) were assessed daily and smoothed using cubic splines, with virus particle count divided by 1000 to match the scale of the host observations. (**B**) Phenotypic evolution of resistance (green) i.e. the proportion of virus populations from all time points a host is resistant to, with circle size corresponding to the number of clones with the same phenotype and of infectivity (orange) i.e. the proportion of host individuals a virus population can infect. Dotted lines represent the maximum range per time point that was maintained at consecutive time

points. Assays were done for 1210 comparisons of ten host clones and one virus population collected from eleven time points. (**C**) Binary visualization of the phenotypic interaction, with orange indicating a phenotypic match and green indicating a mismatch. (**D**) Viral allele frequency trajectories of all derived SNPs that reach a frequency of at least 5% at more than one time point (**E**) Host allele frequency trajectories of all derived SNPs that reach a frequency of at least 25% at more than one time point.

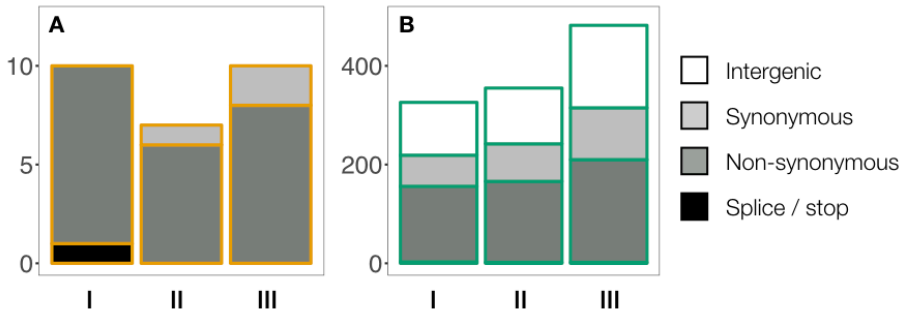

Fig. 2. Molecular evolution differs between virus and host populations. Overall number of observed genetic changes of virus (**A**) and host (**B**) populations colored by the predicted severity of their effect on protein structure (phenotype). Intergenic regions cover 21% and 74% of the virus and host reference genomes, respectively. Bars correspond to the three replicate experiments.

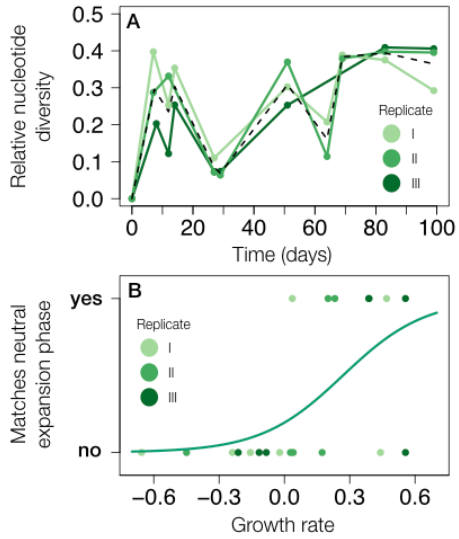

Fig. 3. Dynamics of host genetic diversity show selective sweeps at days 27 and 64. (**A**) Nucleotide diversity was calculated per time point, using derived allele frequencies of all loci that exhibited variation over the time course of the experiments. Lines are colored by replicate, with the black dashed line indicating the average. (**B**) Indicator variable reflecting if the host genetic site frequency spectrum matched the expectations of a neutral expansion phase (Luria-Delbrück-model) plotted against population growth in the three days leading up to the corresponding time point. Every dot reflects a time point and is colored by replicate, the line corresponds to a generalized linear model fit with replicate as random effect.

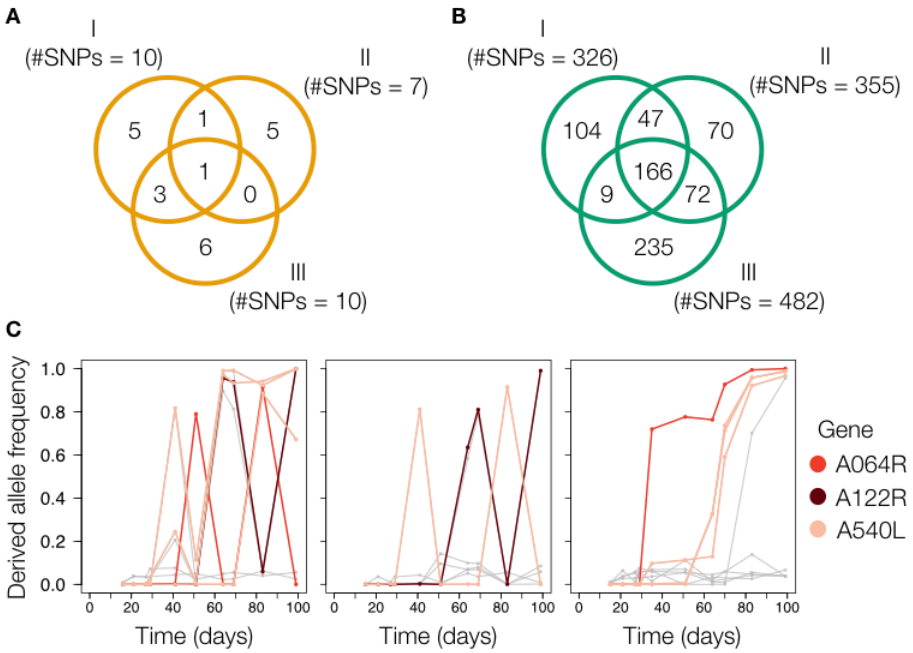

Fig. 4. Repeatable genomic change provides evidence for the action of natural selection. Venn diagrams displaying the number of mutations (SNPs) and the amount of repeatability in virus (**A**) and host (**B**) populations. A mutation was classified as repeated only when the same base change occurred at the same reference position. (**C**) Viral derived allele frequency trajectories, colored by the gene in which they occur if they were repeatedly found. Grey lines reflect trajectories of mutations observed in one replicate only.

Science
AAAS

Supplementary Materials for

The feedback between selection and demography shapes genomic diversity during coevolution

Cas Retel†, Vienna Kowallik†, Weini Huang, Benjamin Werner, Sven Künzel, Lutz Becks‡, Philine G.D. Feulner*‡

* Correspondence to: philine.feulner@eawag.ch

This PDF file includes:

Other Supplementary Materials for this manuscript include the following:

Materials and Methods

Chemostat experiments

Experiments were performed in continuous flow-through systems (chemostats) as previously described (*28*) but using 1000 ml glass bottles containing 800 ml modified BBM (Bold's basal medium with nitrate being replaced by equal moles of ammonium chloride). Sterile medium was continuously supplied to the chemostats at a rate of 0.1 per day. Chemostats were continuously mixed by stirring and maintained at 20°C under light conditions. Chemostats were inoculated from the same liquid culture derived from a single algal clone so that all algal host populations started from the same ancestor. Isogenic virus was added at day 12 to all chemostats.

Algal and virus densities were assessed daily. Algal samples were fixated with 2.5% Lugol for later algal quantification using imaging flow cytometry (FlowCam, Fluid Imaging Technologies, Inc.). For virus enumeration, samples were fixated with 1% glutaraldehyde, flash frozen in liquid nitrogen and stored at -80° C. Virus particles were counted using flow cytometry (FACS Calibur, Becton Dickinson, San Jose, California) following (*36*) and (*28*). In regular intervals, algal and virus subpopulations were preserved for subsequent phenotyping (see (*28*) for details). Simultaneously, 40 ml were taken from each chemostat, concentrated using ultracentrifugation at ~35 000g for 2 hours and the pellet was frozen at -80 °C for DNA extractions.

Log-transformed population sizes of both species were smoothed using cubic splines (spline function in R (*37*)). We tested parallel changes in host population sizes across replicates using wavelet coherence analysis as previously described (*17*). Briefly, we measured the local correlation between two time series and identified the dominant and significant phase shifts between them (*38*, *39*). The value of wavelet coherence is '0' when there is no relation between

the two oscillations (no phase coupling) and '1' when there is a full correlation (perfect phase coupling) between the two oscillators. We extracted from these analyses the significant phase shifts (alpha < 0.05 and outside the cone of influence). Statistical significance of the empirical correlation between replicates was assessed by testing the null hypothesis of absence of correlation with the WaveletComp R package, which allows for simulation of white noise (default methods) (*39*). We restricted analysis to the time period from day 0 till day 55, as algal populations stabilized after this.

Phenotypic assays

To follow the coevolution of resistance and infectivity of host and virus, eleven time points were selected based on population size dynamics. The sampling was aimed to capture each round of growth and decline during the Arms Race phase and decreased in density during the Fluctuating Selection phase. For each time point, ten algal clones were randomly isolated from previously plated populations on agar plates and re-grown in BBM medium. Afterwards, each host clone (110 in total) was exposed to virus populations from all time points, resulting in a total of 1210 growth assays per replicate. To determine the resistance or susceptibility of the algal clones towards the virus populations, their growth when exposed to virus (initial multiplicity of infection MOI of 0.01) was compared to the growth of the algal clone in the absent of the virus. Growth rates were calculated based on optical density measurements (Tecan, Infinite M200PRO, 680 Männedorf, Switzerland) measured at time point 0 and after 72 hours. A host clone was deemed susceptible when the mean growth rate plus two standard deviations of four technical replicates in presence of the virus was lower than mean growth rate minus two standard deviations of the control, or when mean growth rate in presence of the virus was negative. Based on these data resistance and infectivity ranges were calculated. Growth rates of

algal clones measured in the absence of virus were correlated to resistance range to estimate trade-offs between resistance and growth rates. We defined phenotypic match and mismatch periods based on maximum resistance and infectivity range over time, but took only observations into account when the phenotype was maintained in the next time step. If maximum resistance was lower than or equal to infectivity, periods were classified as phenotypic match.

Sequencing design

DNA was extracted from frozen and concentrated samples using the DNeasy Blood and Tissue Kit (Qiagen) with minor modifications. First, 100 µl buffer ATL + 30 µl Proteinase K were added to 200 µl concentrated sample, followed by an incubation at 56°C for 4 hours, continued by adding 600 µl 1:1 buffer AL + Ethanol mix and proceeding by following the standard column-based protocol. Eleven time points from two replicates of coevolution were sequenced on five runs of an Illumina NextSeq (Illumina Nextseq 500 high output) machine. Paired-end libraries were prepared using a NexteraXT library preparation kit. The amount of DNA obtained for host and virus was correlated to their relative population sizes, which for some time points led to comparatively low genome-wide coverage for the host. A sixth NextSeq run was performed to mitigate this issue and increase coverage for a subset of time points.

Read processing

Quality of the reads was assessed using FastQC. For some runs, for which base calling qualities dropped significantly towards the end of the reads, read tails were trimmed using Trimmomatic v0.35 (*40*) with default settings. We ran SeqPrep v1 (https://github.com/jstjohn/SeqPrep) to merge read pairs in case forward and reverse reads overlapped and subsequently remove reads shorter than 70 bp. Reads were mapped with bwa mem v0.7.12 with slightly increased accuracy setting (-r 1) (*41*), to one reference genome

consisting of both host (*42*) and virus (*34*) reference sequences. We ran Picard (v2.0.1) FixMateInformation and AddOrReplaceReadGroups (http://broadinstitute.github.io/picard.), removed alignments with quality 0 with awk, merged data per time point (across lanes and sequencing runs) using samtools v1.3 (*43*). Resulting .bam files containing aligned reads per time point were sorted, cleaned and indexed with Picard SortSam, Picard CleanSam and samtools index. For the virus, average genome-wide coverage was >1000X at all time points where virus was present. We used samtools view with the -s parameter to downsample to an average per-position coverage of 1000X; this makes the subsequent analysis less computationally demanding but keeps the empirical coverage distribution intact for later filtering. Table S1 summarizes average coverage of host reads after quality control and alignment for every time point per replicate. If average per-position coverage was below 10X, the time point was completely removed from analysis. Coverage for specific sites was evaluated after .bam files were transformed to .sync format with samtools mpileup and Popoolation2 (*44*) v1.201 mpileup2sync.pl (--min-qual 1). In these .sync files, sites with a coverage outside of the interval (mean±3 standard deviations) or smaller or equal to 10X were set to NA with a custom R script. The frequency of the non-reference allele with the highest average frequency across time points was calculated as derived allele frequency.

Variant calling and locus filtering

We applied several criteria to (remove sequencing errors, reduce technical artifacts and) obtain only those alleles with patterns driven by selection, following other genomic time-series analyses (*20*, *24*, *45*) unless there was reason to deviate. It is inherent to pooled sequencing data that low-frequency mutations are difficult to distinguish from sequencing errors (*46*). To remove any observed variation induced by sequencing error, we set a conservative coverage-based

detection limit threshold of 5% (virus) and 25% (algae). For any indel calls passing this threshold, all information 10 bp up- and downstream (including the position itself) was not included for further analysis. Because we start the experiments with clonal populations, any observed variation at time point 0 (< 99% ancestral allele frequency) is likely an artefact, and these loci were removed from the dataset. Loci were also removed if the number of missing values exceeded 1 (virus) or 3 (host). Finally, we only include a locus if derived allele frequency reached the detection threshold at more than one time point. In the host datasets, we observed several sets of mutations at closely neighboring reference positions with highly correlated frequency trajectories. Our setup does not permit us to ascertain if those are multiple independent polymorphisms in the same cohort or a larger structural variant that appears as multiple Single Nucleotide Polymorphisms (SNP) in our alignment. Hence SNPs within 1000 bp of each other and with highly correlated frequency trajectories were collapsed into one. Frequency values were averaged and during annotation, the most severe phenotypic effect was used as representative for such collapsed sets. Because we expect selection to be non-constant under the described dynamic eco-evolutionary circumstances, we did not filter allele frequency trajectories for lack of temporal autocorrelation. Table S2 shows the number of allele frequency trajectories removed by each filtering step. The final set of SNPs was annotated using snpeff (*47*).

Given the observed population sizes and length of the experiment, it is highly unlikely for spontaneously arising neutrally evolving loci to reach the detection limit by drift alone (*48*). Any allele that reaches a detectable frequency is therefore either under positive selection or linked to something that is (*49*). We acknowledge that because we rather stringently filter for potential sequencing errors, we inevitably also exclude low-frequency genomic variation from analysis, thus do not exhaustively characterize the genomic variation in the populations. Because both host

and virus populations are not known to recombine, this temporal genome-wide SNP dataset provides an accurate image of the strength and speed of evolution.

Genetic diversity in an expanding population

In an exponentially growing population, *de novo* variants can rapidly increase in number. If all individuals (cells) have comparable growth rates (i.e. when apparent fitness differences are absent), the expected site frequency spectrum generated by the underlying stochastic process of *de novo* mutation follows a Landau distribution (*32*), first detected in the famous Luria-Delbrück experiment (*50*). Specifically, the number of variants present within a set of cells decreases proportionally to the number of cells squared, and thus the probability $P(n_f)$ to have a certain number of variants n at a given frequency f is

$$P\ (n_f) \sim \frac{1}{f^2}$$

Therefore, the cumulative number of variants M_f with frequency smaller or equal to a certain frequency f is proportional to the inverse of f:

$$M_f \sim \frac{1}{f}$$

We plotted the cumulative number of variants M_f against the inverse of the frequency $1/f$, excluding variants with a frequency below 5% because variance induced by sequencing increases with decreasing minor allele frequency, and at such low frequencies could distort the empirical power dependency expected under neutrality. If the variants were generated by random *de novo* mutation during an expansion phase without fitness differences between individuals, these points should fall onto a straight line. We applied a linear regression to quantitatively assess this and

separated time points based on the obtained R^2 values, with $R^2 > 0.9$ matching the expectation of a neutral expansion phase. Results for every time point and replicate are provided in Fig. S5.

Considering a selective sweep, when a single highly adaptive cell grows exponentially, then to reach a frequency of 10% by hitchhiking alone, any neutral mutation needs to occur during the first ten cell division this cell undergoes. This means that with a genome size of ~42 Mb, observing power law dependencies and rapid neutral allele frequency increases of 10% during sweeps are feasible if the *Chlorella* mutation probability is around $1 / (42*10^6 * 10) = 2.4 * 10^{-9}$ substitutions / position / cell division. While there are no good estimates of the mutation rate in *Chlorella*, such a rate is plausible. As the virus genome is orders of magnitude smaller (~330 Kb), observing comparable power law dependencies would require a mutation rate of $1 / (330 * 10^3 * 10) = 3.0 * 10^{-7}$ substitutions / position / cell division. Such rates have been observed for DNA viruses. However, small virus genomes are densely packed and neutral positions are likely rare.

We performed a logistic regression of time points with reduced genetic diversity (also those where the site frequency spectrum matched the expectation under neutral expansion) on host population growth (Generalized Linear Model with random effect, family = binomial) using the R package lme4 (*51*). We only included days when virus was present and averaged growth over the 3 days leading up to the time point of genetic sampling. Replicate was included as random effect to account for within-replicate dependency of data points.

Probability of observing the same SNP in multiple replicates

Assuming that mutations evolve *de novo*, are neutral, and uniformly distributed across the genome, every genomic position has the same probability of acquiring a mutation. Under these assumptions, observing a mutation in our experiments is equivalent to randomly drawing

marbles from a vase without replacement. The size of the vase is equivalent to the number of genomic positions we evaluate with our sequencing approach, and the sample size (number of marbles drawn) equals the number of mutations observed per replicate. To assess how likely the empirically observed overlap is, we simulated such a sampling procedure using R and find that the probability of the observed overlap (Fig. 4A,B) is extremely small ($p < 10^{-5}$). Due to i.a. random variation in sequencing coverage and complex genomic regions, not every position of the reference genome can be reliably evaluated, hence reference genome size is an overestimate of vase size. To get an idea of how large the pool of mutable sites needs to be to reproduce the empirically observed overlap, we repeated the simulations for a grid of vase sizes, using the empirical number of observed mutations (minimum across three replicates) as the total number of marbles drawn and report the number of marbles drawn more than once (i.e. SNPs observed in multiple replicates) in Table S2.

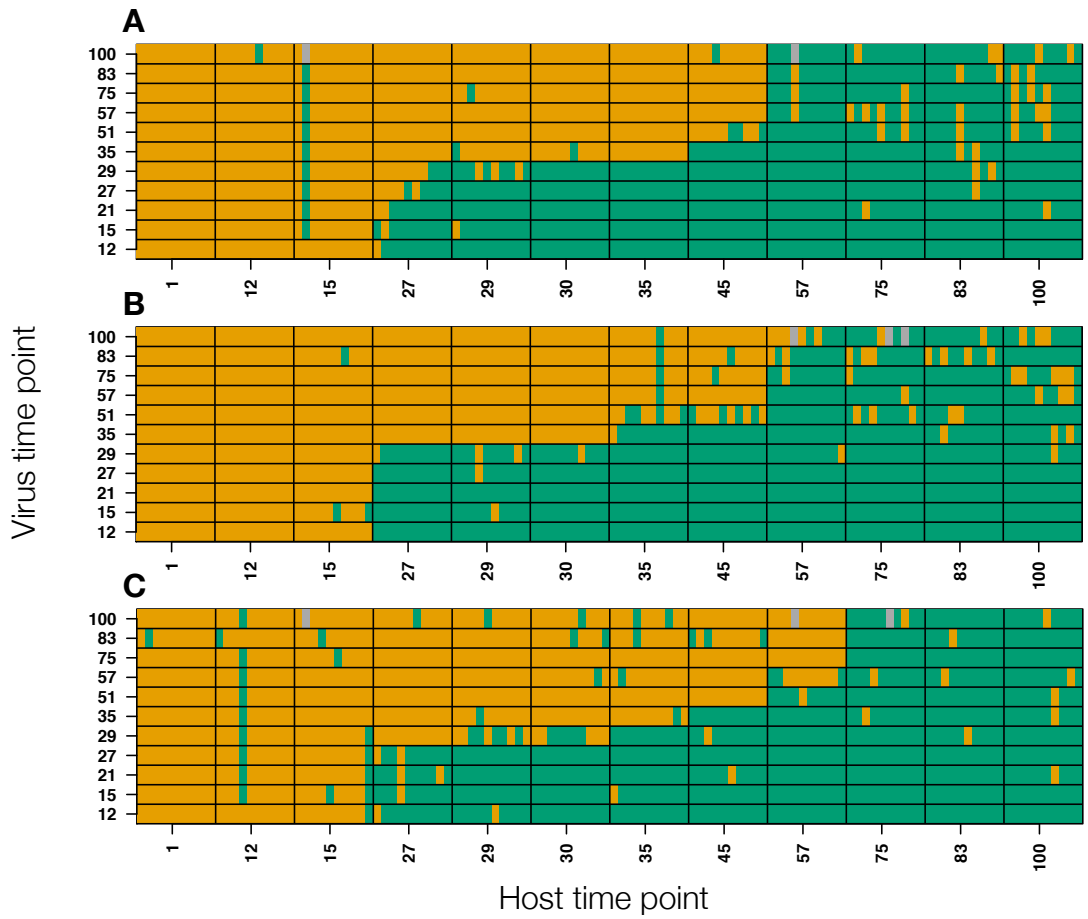

Fig. S1. Full infection matrix highlights co-evolutionary phenotypic changes. For each pairwise combination of time points (black outlined rectangles) ten host clones (horizontal axis) and one virus population (vertical axis) were tested in comparative growth assays. Green squares (inside each of the boxed rectangles) indicate that the host clone was resistant, orange squares indicate host was susceptible to infection by the virus. Assays compared host growth in absence versus presence of virus across four technical replicates. If mean plus two standard deviations of growth in presence of the virus did not overlap with mean minus two standard deviations in absence, or if average growth in presence of the virus was negative, the host was deemed susceptible. Figures **A**, **B** and **C** correspond to replicates I, II and III, respectively.

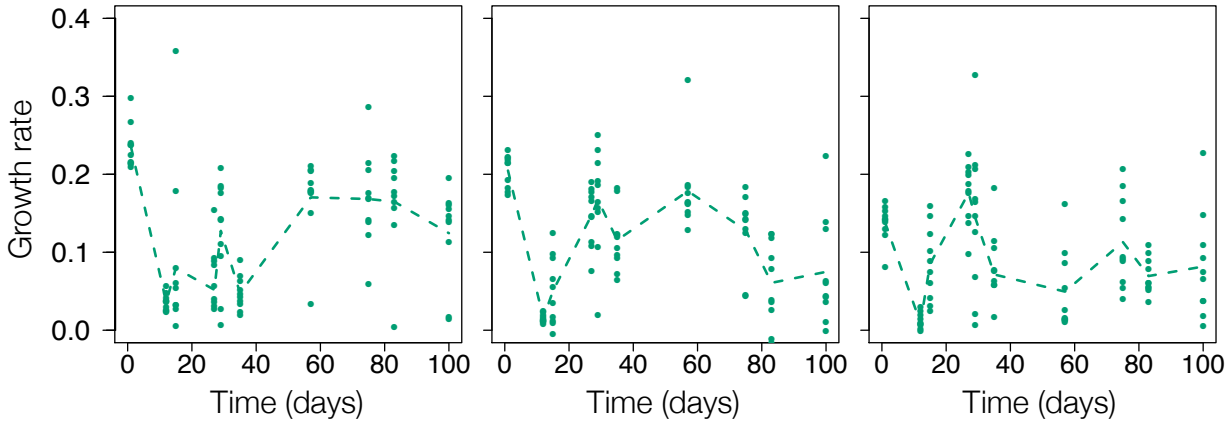

Fig. S2. Host fitness does not monotonically increase over time. Plotted are growth rates of ten host individuals in the presence of contemporary virus, i.e. fitness, per time point. Dashed lines reflect the change in average growth rate, which is equivalent to population performance. Growth rates measured at day 0 are in absence of any virus. As opposed to increasing performance over time, during antagonistic co-evolution host populations adapt in accordance with Van Valen's Red Queen hypothesis (*52*) and average fitness shows alternating increases and decreases. The three panels correspond to three replicate experiments.

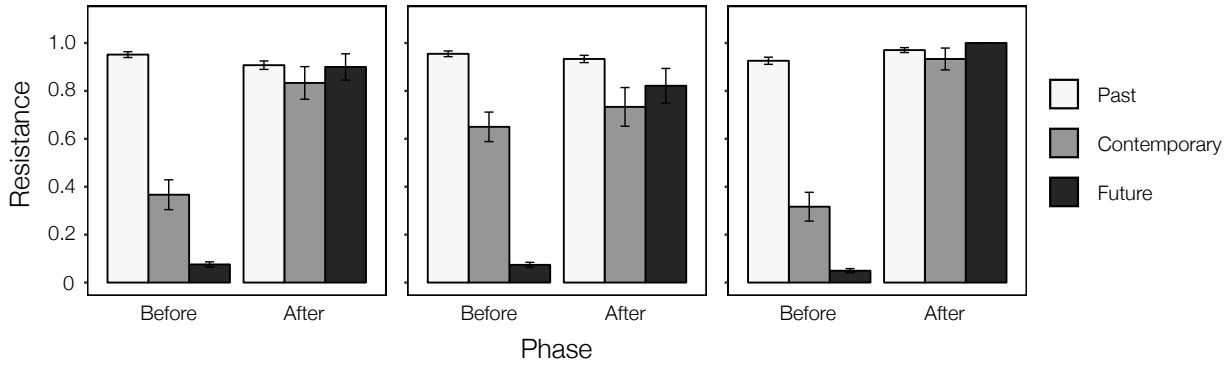

Fig. S3. Phenotypic data show a shift from Arms Race to Fluctuating Selection dynamics. Plotted are means of multiple host resistance assays for time points before or after the generalist was first observed (Days 57, 57 and 75 in replicates I, II and III, respectively). Greyshades indicate the relative time point of the virus used in the assay, i.e. whether it came from an earlier, the same or a later time point. Error bars represent the standard error of the mean (binomial distribution). Before occurrence of the generalist, hosts were on average more resistant to viruses from previous time points and mostly susceptible to viruses from later time points (generalized linear model per replicate with resistance as binomial response and comparison as explanatory variable with contemporary as baseline yielded p-values of $2.34*10^{-10}$ or smaller; no multiplicity correction applied), which is the predicted pattern of phenotypic change under Arms Race dynamics. After the evolution of a generalist, average resistance of host clones tested against viruses from previous, contemporary and later time points stops increasing (same model, one significant difference found between previous and contemporary comparisons in replicate II, with a p-value of 0.00069; no multiplicity correction applied), as expected under Fluctuating Selection dynamics. Panels show results for replicate I, II, and III.

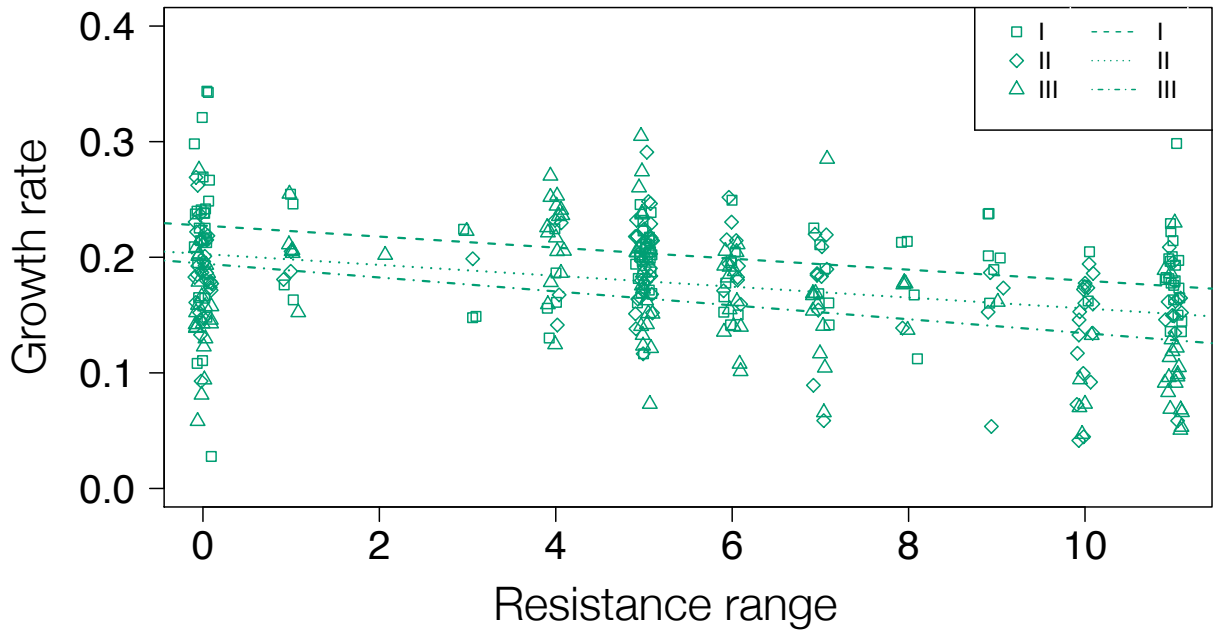

Fig. S4. Resistance is costly. For each host population, host growth rate in absence of virus is plotted against resistance range (0 corresponding to susceptibility to virus from every time point, 11 indicating resistance against every virus). Linear regressions of growth rate on resistance range yields negative slope estimates of $5.2*10^{-3} \pm 7.4*10^{-4}$ (p-values always smaller than 0.01) for the three respective replicates; fits are shown as dotted lines. The negative correlation indicates the presence of a tradeoff between resistance range and growth in absence of the virus, which allows maintenance of multiple resistance types in the host population after the generalist evolves (resistance range 10) (*28*). The legend shows symbols and line types used for the three replicate experiments.

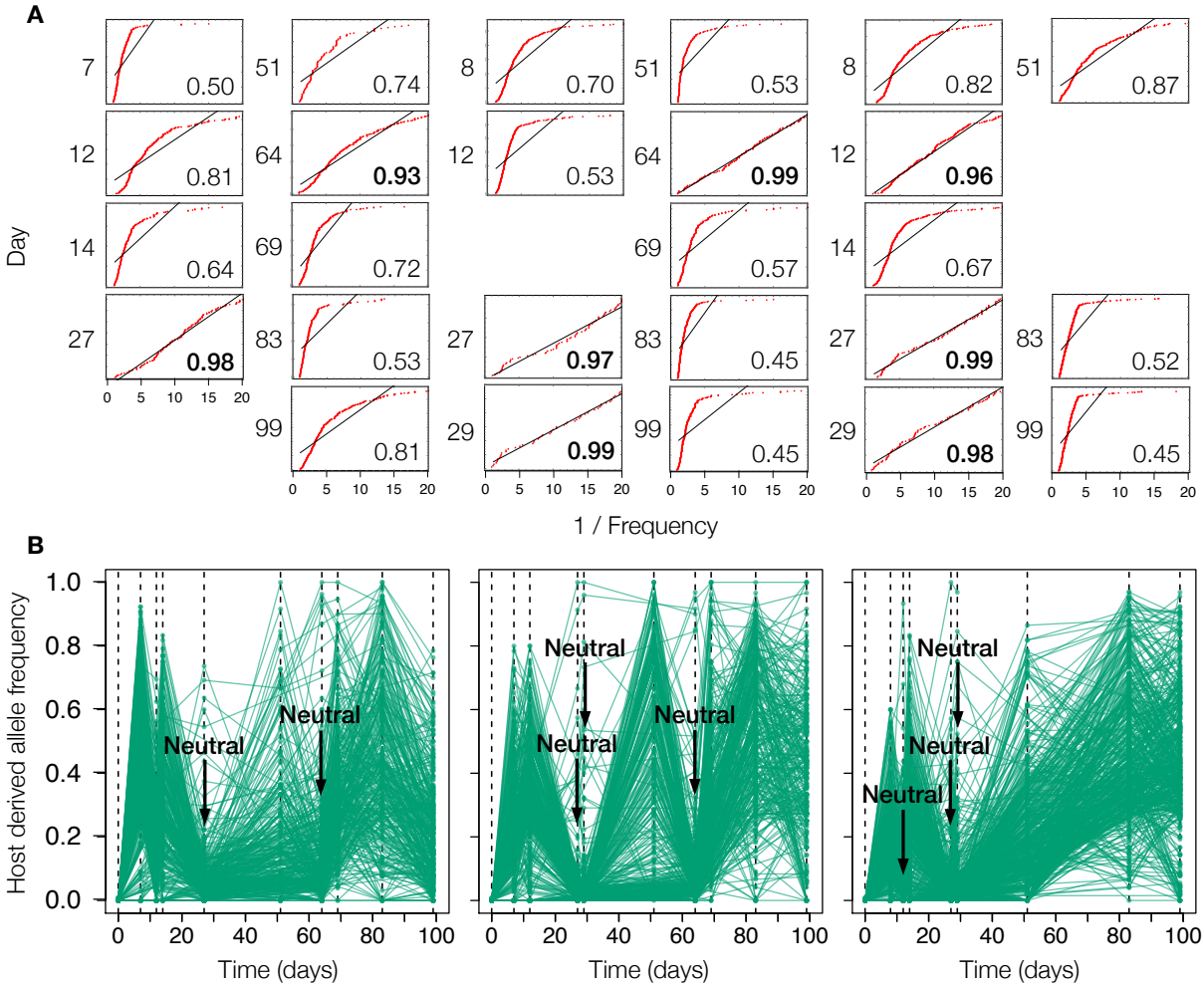

Fig. S5. Genetic diversity after selective sweeps matches expectations under neutrality. (**A**) Derived allele frequencies were ordered by decreasing frequency, and cumulative mutant counts are plotted as red dots against the inverse of the derived frequency. R^2-values of linear regressions through these points are given in the bottom right corners; they are bold when the time point matches the Luria-Delbrück expectation under neutral population expansion (see Methods for more details). (**B**) Derived host allele frequencies per replicate (c.f. Fig. 1E), here with time points matching the Luria-Delbrück model indicated by black arrows. Except for the addition of day 12 in replicate III, these time points are the same as those where selective sweeps

were identified based on a reduction of genetic diversity (Fig. 3A). Panels show results for replicates I, II, and III.

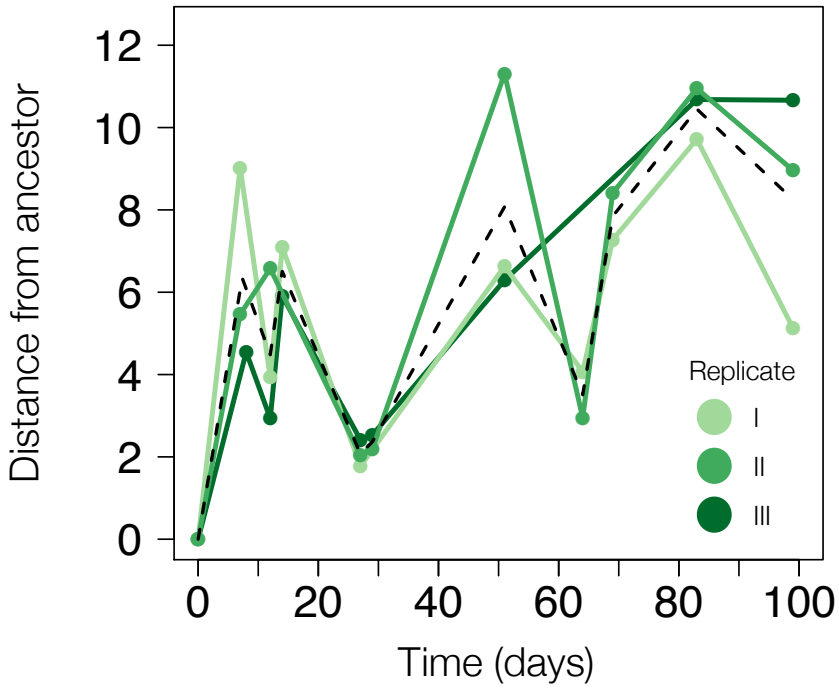

Fig. S6. Genetic distance from the ancestor does not monotonically increase over time. Shown is Euclidean distance between the ancestral host and host populations at every subsequent time point, calculated using derived allele frequencies at all loci that show variation during the experiments. In the process of variation loss during sweeps (Fig. 3A), host populations become more genetically similar to the ancestor. This process was previously described as the "leapfrog" phenomenon (*21*).

A

Day	*0*	*07 08*	*12*	*14 15*	*21*	*27*	*29*	*35 41*	*51*	*64*	*69*	*83*	*99*
I		13	33	13	~~1~~	61	~~1~~	~~0~~	11	39	15	11	40
II		33	45	~~1~~	~~1~~	125	139	~~1~~	8	83	10	13	13
III	39	88	168	52	~~3~~	122	154	~~4~~	28	~~0~~	~~0~~	40	56

B

Filtering step	*1*	*2*	*3*	*4*	*5*	*6*
I	10804	9232	2326	418	384	326
II	9623	8403	2177	470	454	355
IIII	13038	11126	2262	646	636	482

C

Filtering step	*1*	*2*	*3*	*4*	*5*	*6*
I	275	163	34	12	10	10
II	167	133	39	11	7	7
IIII	431	308	81	16	10	10

Table S1. Sequencing and filtering statistics indicate the reliability of the genomic data sets. (**A**) Average depth of coverage for each time point per reference position for host populations after quality control and read alignment. DNA was always extracted for pairs of adjacent days, and sequencing libraries were prepared for the leg (member of each pair) with the highest concentration of DNA; this is why sometimes two days are mentioned per column (e.g. 7 & 8). Because DNA was extracted directly from chemostat samples, coverage per time point is correlated to the ratio of host-to-virus particles present at the time of sampling (see Methods for details). Struck through entries were removed from analysis because of low coverage. Across replicates and time points, virus coverage ranged from 1152X to 60411X (replicate I day 83 and replicate 3 day 21, respectively), and datasets were down-sampled to 1000X for every time point (see Methods for details). (**BC**) Number of polymorphic loci left after each filtering step for host (**B**) and virus (**C**) datasets. Filtering steps: 1 = changes derived frequency by less than 5% (virus) or 25% (host) in the course of the experiments, 2 = within 10 bp of an indel call, 3 = above 1%

derived frequency at first observation, 4 = above detection threshold at only one time point, 5 = has more than 1 (virus) or 3 (host) missing values, 6 = merged frequency trajectory of SNPs with highly correlated frequency trajectories within 1000 bp. Rows indicate the three replicates I, II, and III.

A

n_total	X_obs ± sd
1000	473 ± 7,8
1200	425 ± 8,7
1400	383 ± 9,3
1600	348 ± 9,6
1800	318 ± 9,8
2000	**292 ± 10,1**
2200	270 ± 10,2
2400	251 ± 10,3
2600	235 ± 10,2
2800	220 ± 10,3
3000	207 ± 10,2
5000	130 ± 9,4
10 000	67 ± 7,4

B

n_total	X_obs ± sd
20	10 ± 1,1
50	**5,2 ± 1,5**
100	2,8 ± 1,4
200	1,4 ± 1,1
500	0,60 ± 0,74
1000	0,30 ± 0,54

Table S2. Observing mutations in multiple replicates independently is unlikely under neutrality. Values reflect the number of mutations that were observed multiple times, when randomly inducing the empirical number of mutations in our experiments under stringent assumptions of neutrality, for a grid of sample sizes (Material and Methods). Results most closely matching empirically observed overlap (Fig. 4B,C) for host (**A**) and virus (**B**) are highlighted in bold. The pool of potentially mutable sites needs to be substantially smaller than the *Chlorella variabilis* NC64A and Chlorovirus PBCV-1 reference genomes, which are respectively 42 MB and 56 kB in size and of which our approach allows us to evaluate more than 90% per replicate.

replicate	chromo-some	position	reps found	repeatable day 27	predicted effect	proteinID	Predicted protein	Cellular function (kogClass)
I	6	624455	3	TRUE	non-synonymous	143606	Histone acetyltransferase activity	Transcription
I	25	504343	3	TRUE	intergenic	NA	NA	NA
II	19	680125	2	TRUE	synonymous	36653	NA	NA
II	25	504343	3	TRUE	intergenic	NA	NA	NA
II	28	201721	2	TRUE	intergenic	140025	Ubiquitin-protein ligase	NA
III	6	624455	3	TRUE	non-synonymous	143606	Histone acetyltransferase activity	Transcription
III	19	680125	2	TRUE	synonymous	36653	NA	NA
III	25	504343	3	TRUE	intergenic	NA	NA	NA
III	28	201721	2	TRUE	intergenic	140025	Ubiquitin-protein ligase	NA
III	140	1285	2	FALSE	non-synonymous	NA	NA	NA

Table S3. Functional annotations of SNPs at high frequency in host populations after selective sweep at day 27. Available information on protein structure and function (GO, KOG and KEGG databases) was extracted for all repeatable mutations above 40% frequency at this time point. The "reps found" column represents in how many experimental replicates the mutation was observed, we assigned "repeatable day 27" TRUE when its frequency is repeatedly above 40% at day 27. Two out of five unique SNPs are non-synonymous. Protein 143606 has predicted histone acetyltransferase activity, which potentially affects expression profiles of a wide range of other genes. Like the mutation observed in this gene, most of the other SNPs are not only repeatable, but consistently above 40% frequency at day 27; annotation information however is limited.

replicate	chromo-some	position	reps found	repeatable day 64	predicted effect	proteinID	Predicted protein	Cellular function (kogClass)
I	2	770986	3	FALSE	non-synonymous	49863	NA	Chromatin structure and dynamics
I	3	1038582	3	FALSE	non-synonymous	140596	NA	NA
I	6	247546	3	TRUE	non-synonymous	143495	NA	NA
I	6	247548	2	FALSE	synonymous	143495	NA	NA
I	6	624455	3	TRUE	non-synonymous	143606	Histone acetyltransferase	Transcription
I	10	1373395	3	FALSE	non-synonymous	23149	Dephospho-CoA kinase	Coenzyme transport and metabolism
I	16	1053076	3	FALSE	non-synonymous	58484	Predicted lipase/calmodulin-binding heat-shock protein	Lipid transport and metabolism
I	19	683581	3	FALSE	synonymous	36653	NA	NA
I	32	280834	3	TRUE	non-synonymous	56405	Acyl-CoA synthetase	Lipid transport and metabolism
II	6	247546	3	TRUE	non-synonymous	143495	NA	NA
II	6	624455	3	TRUE	non-synonymous	143606	Histone acetyltransferase	Transcription
II	8	814819	2	FALSE	synonymous	144896	Acyl-CoA synthetase	Lipid transport and metabolism
II	10	4355	2	FALSE	synonymous	52216	Argininosuccinate synthase	Amino acid transport and metabolism
II	12	741075	2	FALSE	synonymous	24126	NA	Protein amino acid phosphorylation
II	20	806812	2	FALSE	non-synonymous	138471	NA	Lipid transport and metabolism
II	26	477054	3	FALSE	synonymous	32953	Ribonucleotide reductase	Nucleotide transport and metabolism
II	32	280834	3	TRUE	non-synonymous	56405	Acyl-CoA synthetase	Lipid transport and metabolism
II	140	1285	2	FALSE	non-synonymous	NA	NA	NA

Table S4. Functional annotations of SNPs at high frequency in host populations after selective sweep at day 64. Available information on protein structure and function (GO, KOG and KEGG databases) was extracted for all repeatable mutations above 40% frequency at this time point. The "reps found" column represents in how many experimental replicates the mutation was observed, we assigned "repeatable day 64" TRUE when its frequency is repeatably above 40% at day 64. Nine out of fifteen unique SNPs are non-synonymous. Eight are in genes encoding proteins involved in metabolism, transporting lipids, amino acids or nucleotides, and two

others have a putative role in regulation of gene expression (chromatin structure and histone acetyltransferase). Though all of these potentially alter cell wall composition, no obvious candidate stands out.

Data S1. Population sizes (observed and smoothed values).

Population size counts for host and virus populations and smoothed values shown in Fig. 1A (.xlsx format)

Data S2. Results of phenotypic assays.

Growth rates for 110 host individuals in presence and absence of 11 virus populations (.xlsx format), used to calculate resistance and infection ranges.

Data S3. Filtered derived allele frequencies.

Derived allele frequency of SNPs meeting our filtering criteria, plotted in Fig. 1DE (.xlsx format).